Optica Applicata, Vol. XLIII, No. 4, 2013
DOI: 10.5277/oa130408

Optical gradient force of cosh-Gaussian with sine-azimuthal and half-space phase modulation

RUI FU[1*], XIUMIN GAO[1, 2], HAIBIN SHEN[3], QING XIN[1], XINMIAO LU[1], LINGWEI GUO[1]

[1]Electronics & Information College, Hangzhou Dianzi University, Hangzhou 310018, China

[2]Key Laboratory of RF Circuit and System (Hangzhou Dianzi University), Ministry of Education, Hangzhou 310018, China

[3]China Jiliang University, Hangzhou 310018, China

[*]Corresponding author: fu2008rui@126.com

The optical gradient force distributions in focal plane of cosh-Gaussian beams with sine-azimuthal variation wavefront and half space phase modulation were investigated. Results show that optical gradient force distributions can be affected considerably by the phase retardation of half-space phase modulation, of a phase parameter that indicates the phase change frequency on an increasing azimuthal angle, and beam parameters in cosh terms of the incident beams. Many gradient force patterns occur, including cross-shape, multiple optical trap arrays, multiple-trap wheel, and many kinds of gradient force lines and curves. Symmetry of the whole gradient force pattern can also be altered remarkably. Above results may find wide applications in optical trapping systems.

Keywords: optical gradient force, cosh-Gaussian beams, wavefront modulation.

1. Introduction

Optical gradient force plays an important role in some systems, especially in the optical trapping technique [1–3]. Optical trapping systems have accelerated many major advances in numerous areas of science [4–7], including force detection measurement [8], micro-machine and micro-component [9], microscopy [10], in life science, optical tweezers can offer a very convenient, noninvasive, and non-contact access to processes at the microscopic scale [11]. In optical trapping systems, it is usually deemed that the forces exerted on the particle in the light field consist of two kinds of forces. One is the optical gradient force, which plays a crucial role in constructing an optical trap and its intensity is proportional to the optical intensity gradient; the other kind of force is the scattering force, which usually has complex forms because

this kind of force is related to the properties of the trapped particles, and whose intensity is proportional to the optical intensity [12]. The optical gradient force is necessary for optical trapping, therefore, the construction of tunable gradient force patterns is very important and attracts many researchers [13–16]. Recently, the optical gradient force has also been used in a tunable optical coupler [17].

On the other hand, cosh-Gaussian beams have attracted much attention because their profiles can be altered by choosing the suitable decentered parameters in cosh parts [18, 19], and their propagation and focusing properties have become the object of many works [20–23]. In addition, self-focusing of cosh-Gaussian beams has also been investigated [24, 25]. Recently, an optical vortex has also been introduced in cosh-Gausain beams, and corresponding focusing properties have been investigated theoretically [26–30]. However, to our knowledge, the gradient force patterns of sine-azimuthal wavefront-modulated cosh-Gaussian beams by half-space phase modulation have not been investigated to date, so, this article focuses on the gradient force patterns. The principle of the gradient force patterns of cosh-Gaussian beams is given in Section 2. And Section 3 shows the simulation results and discussions. The conclusions are summarized in Section 4.

2. Gradient force calculation of the focusing system

In the system we investigated, the gradient force can be expressed as [12]

$$F_{\text{grad}} = \frac{n_b^2 r^3}{2}\left(\frac{T^2-1}{T^2+2}\right)\nabla\left|\mathbf{E}(\rho, \psi, z)\right|^2 \tag{1}$$

where r is the radius of particles, n_b is the refraction index of the surrounding medium. And the parameter T, the relative index of refraction, is equal to the ratio of the refraction index of the particle n_p to the refraction index of the surrounding medium n_b. Gradient force F_{grad} points in the direction of the gradient of the light intensity if the diffractive index of particles is bigger than that of surrounding medium, *i.e.*, $n_p > n_b$. In the next section, the gradient force pattern is investigated numerically basing on Eq. (5), and the gradient forces patterns are illustrated to show their promising applications in constructing a tunable optical trap. $\mathbf{E}(\rho, \psi, z)$ is the electric field in the focal region. According to the vector diffraction theory [31, 32], the amplitude of electric field in the focal region can be written as,

$$\mathbf{E}(\rho, \psi, z) = \frac{1}{\lambda}\int_0^{\alpha}\int_0^{2\pi} E(\theta, \varphi)(C_1\mathbf{x} + C_2\mathbf{y} + C_3\mathbf{z})C_4 \mathrm{d}\theta\,\mathrm{d}\varphi \tag{2}$$

where

$$C_1 = \cos(\theta) + \sin^2(\varphi)\left[1 - \cos(\theta)\right]$$

$$C_2 = \cos(\varphi)\sin(\varphi)\left[\cos(\theta) - 1\right]$$

$$C_3 = \cos(\varphi)\sin(\theta)$$

$$C_4 = \exp\left[-ik\rho\sin(\theta)\cos(\varphi-\psi)\right]\exp\left[-ikz\cos(\theta)\right]\sin(\theta)$$

and $\varphi \in [0, 2\pi)$, $\theta \in [0, \alpha]$, $\alpha = \text{asin(NA)}$, where NA is the numerical aperture of the optical focusing system. Vectors **x**, **y**, and **z** are the unit vectors in the x, y, and z directions, respectively. It is clear that there are three components (E_i, E_j and E_k) in x, y, and z directions, respectively. The variables ρ, ψ, and z are the cylindrical coordinates of an observation point in the focal region. $E(\theta, \varphi)$ is the amplitude of electric field of the sine-azimuthal wavefront-modulated cosh-Gaussian beam in radial coordinates by half-space phase modulation, and can be expressed as,

$$E(\theta, \varphi) = A_0 C_5 C_6 C_7 \tag{3}$$

where A_0 is a constant, and

$$C_5 = \cosh\left[\text{NA}^{-1}\beta_x\sin(\theta)\cos(\varphi)\right]$$

$$C_6 = \cosh\left[\text{NA}^{-1}\beta_y\sin(\theta)\sin(\varphi)\right]$$

$$C_7 = \exp\left[-\frac{\sin^2(\theta)}{\text{NA}^2 w^2}\right]\exp\left[-i\pi\sin(m\varphi)+i\varphi_0\right]$$

while m is the phase factor of the wavefront phase modulation, $w = \omega_0/r_p$ is called as the relative waist width, ω_0 is the waist width (defined as radius) of the incident cosh-Gaussian beam, and r_p is the radius of the optical aperture. The parameters β_x and β_y are called the decentered parameters of the cosh-Gaussian beam, and the phase change induced by the phase plate is,

$$\varphi_0 = \begin{cases} 0, & \varphi \in [0, \pi) \\ \delta, & \varphi \in [\pi, 2\pi) \end{cases} \tag{4}$$

where δ is half-space phase retardation of the kind of cosh-Gaussian beams. It is assumed that the cosh-Gaussian beam is linearly polarized along the x axis. By substituting Eq. (3) into Eq. (2), the electric field in the focal region is rewritten as,

$$\mathbf{E}(\rho, \psi, z) = \frac{A_0}{\lambda}\int_0^{\alpha}\int_0^{2\pi} C_5 C_6 C_7 (C_1\mathbf{x} + C_2\mathbf{y} + C_3\mathbf{z}) C_4 \,\mathrm{d}\theta\,\mathrm{d}\varphi \tag{5}$$

Therefore, substituting Eq. (5) into Eq. (1), we can obtain the optical gradient force pattern in the focal plane of the kind of cosh-Gaussian beams by calculating numerically Eq. (1).

3. Numerical results and discussions

It should be noted that the distance unit in all figures is the wavelength of an incident beam in vacuum, and the arrows in figures indicate the direction of the optical gradient force. Firstly, the optical gradient force patterns under condition of lower numerical aperture were investigated. Without the loss of generalization and validity, the numerical aperture is chosen as NA = 0.4, and $\beta = \beta_x = \beta_y = 1$. Figure 1 illustrates the gra-

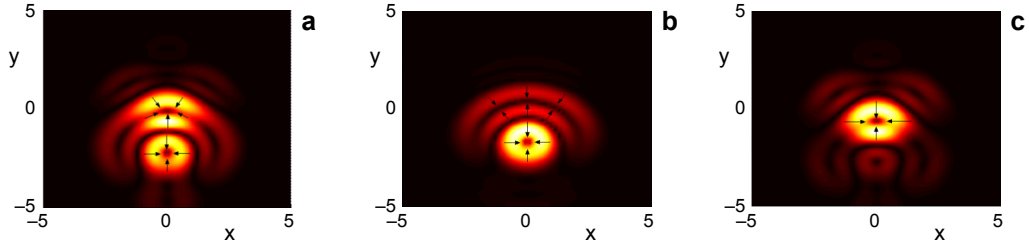

Fig. 1. Gradient force distributions under condition of NA = 0.4, $\beta = 1$, $m = 1$, and $\delta = 0$ (**a**), $\delta = \pi/2$ (**b**) and $\delta = \pi$ (**c**).

dient force patterns under condition of $m = 1$ and different phase retardation δ of the half-space phase modulation. It can be seen that there are one main circular optical trap and one weak crescent-shape optical trap for the case of $\delta = 0$. On increasing δ, the whole gradient force pattern shifts along y axis, and the main circular trap weakens and the weak crescent-shape optical trap gets stronger and stronger, as shown in Fig. 1**b**. When the value of phase retardation δ increases up to π, the previous circular optical trap becomes very weak. Simultaneously, the crescent-shape optical trap has evolved into one main circular optical trap, as given in Fig. 1**c**. From above gradient force pattern evolution process, we can see that the effect of the phase retardation δ on the gradient force pattern in the focal plane is very considerable, and the position and shape of the gradient force pattern can be altered by δ.

Figure 2 gives the gradient force distributions for the case of $m = 2$ and other parameters are the same in Fig. 1. When the phase factor increases from 1 to 2, the whole gradient force pattern changes remarkably by comparing Fig. 2 with Fig. 1.

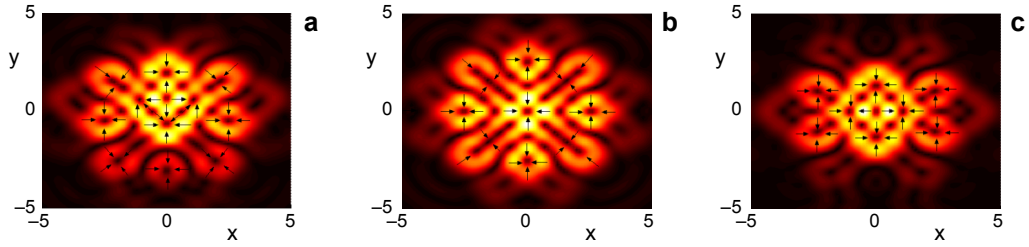

Fig. 2. Gradient force distributions under condition of NA = 0.4, $\beta = 1$, $m = 2$, and $\delta = 0$ (**a**), $\delta = \pi/2$ (**b**) and $\delta = \pi$ (**c**).

Under condition of $\delta = 0$, there is one cross-shape gradient force pattern with four optical traps between those branches of the center cross-shape gradient force pattern, and the main trap locates at the center point, as shown in Fig. 2**a**. On increasing the phase retardation δ, the gradient force in the negative half-space of the y axis weakens considerably, and at the same evolution process, the whole gradient force pattern shifts along y axis. When δ increases up to π, the whole gradient force pattern changes back to symmetrical about x and y axis, and one center main trap with four outside overlapping traps comes into being, as illustrated in Fig. 2**c**. It can be seen that the effect of the phase factor on the gradient force pattern is also considerable.

Now, we increase the value of m continuously, and the gradient force pattern turns on Y shape for the case of $\delta = 0$ and $m = 3$, as shown in Fig. 3**a**. There is one main circular optical trap at the center point, and three trap lines also come into being outside the radial direction. The whole gradient force pattern is like a triangle shape. On increasing δ, the whole gradient force pattern shifts along y axis, and the outside three trap lines weaken considerably. When the value of the phase retardation δ equals π, there remains only one main circular optical trap, as shown in Fig. 3**c**.

Here, the optical gradient force distributions in the focal plane under condition of $m = 4$ are given in Fig. 4. The gradient force pattern is very symmetric for the case of $\delta = 0$, there is one center main trap, and also eight circular weak traps and eight circular weak trap lines appear outside, which turn on the trap's wheel. On increasing the value of δ, the gradient force patterns of this kind change very remarkably, and the symmetry about y axis is disturbed, as shown in Fig. 4**b**. At the same evolution

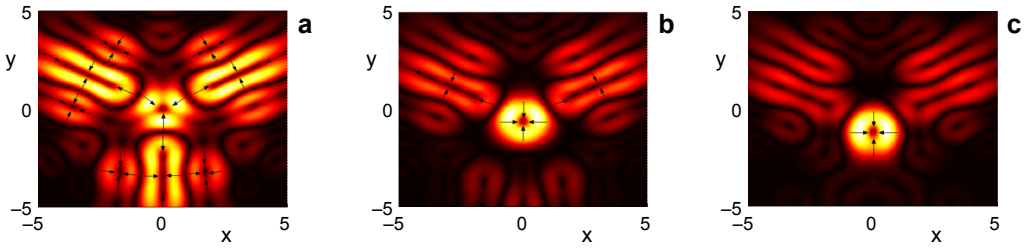

Fig. 3. Gradient force distributions under condition of NA = 0.4, $\beta = 1$, $m = 3$, and $\delta = 0$ (**a**), $\delta = \pi/2$ (**b**) and $\delta = \pi$ (**c**).

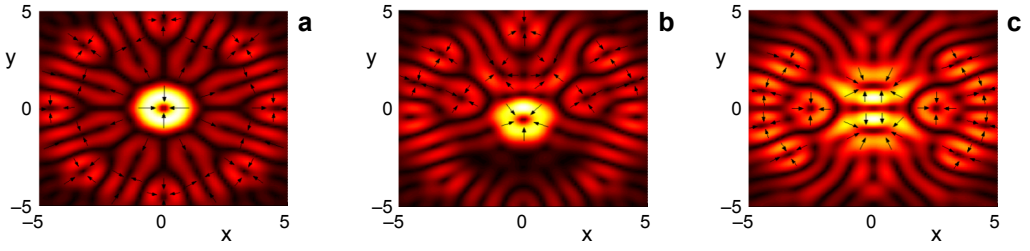

Fig. 4. Gradient force distributions under condition of NA = 0.4, $\beta = 1$, $m = 4$, and $\delta = 0$ (**a**), $\delta = \pi/2$ (**b**) and $\delta = \pi$ (**c**).

process, the center circular gradient force pattern also distorts very considerably. When δ increases up to π, two distorted optical traps come into being with many weak traps outside, as illustrated in Fig. 4**c**.

In order to get a deep insight into the optical gradient force evolution, the value of a phase factor was increased up to $m = 5$, and some gradient force patterns are shown in Fig. 5. The gradient force pattern turns on one center circular trap with five branches outside the radial direction under condition of $\delta = 0$, as shown in Fig. 5**a**. On increasing δ, the whole gradient force pattern changes, especially the part in the negative side of y axis. Namely, the gradient force below the main gradient force trap weakens very considerably, and symmetry of the whole gradient force pattern also distorts. When the value of δ increases up to π, the gradient force pattern becomes symmetric only about y axis, and the center trap distorts in y coordinate direction, as given in Fig. 5**c**.

From the above gradient force pattern evolution, we can see that the effect of the phase retardation and the phase factor on the optical gradient force is very considerable. And the symmetry of the gradient force pattern also changes remarkably in the same evolution process. In addition, the symmetry is related closely to the phase factor, though, the whole gradient force pattern turns on a star-shape with different branches in the radial direction, when the phase factor is an odd number, and the number of branches equals the phase factor. When the phase factor is an even number, the number of branches is two times the phase factor, and higher phase retardation will distort considerably this kind of symmetry properties.

Here, we investigate the effect of higher decentered parameters on the gradient force pattern evolution. The gradient force is calculated under condition of $\beta = \beta_x =$

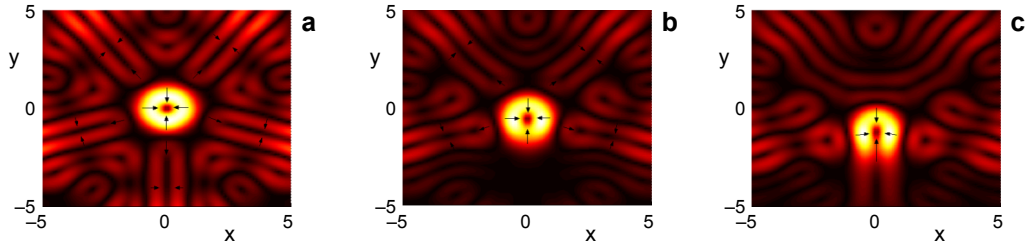

Fig. 5. Gradient force distributions under condition of NA = 0.4, $\beta = 1$, $m = 5$, and $\delta = 0$ (**a**), $\delta = \pi/2$ (**b**) and $\delta = \pi$ (**c**).

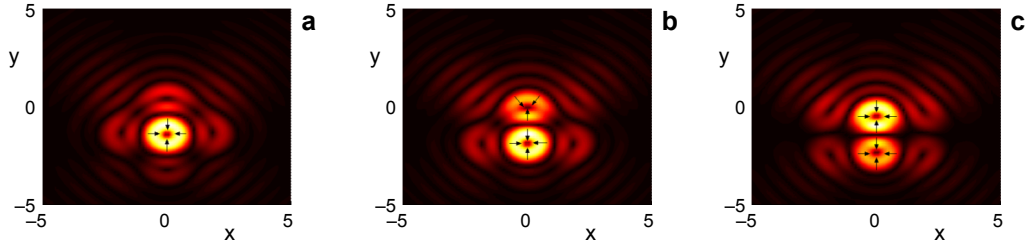

Fig. 6. Gradient force distributions under condition of NA = 0.4, $\beta = 5$, $m = 1$, and $\delta = 0$ (**a**), $\delta = \pi/2$ (**b**) and $\delta = \pi$ (**c**).

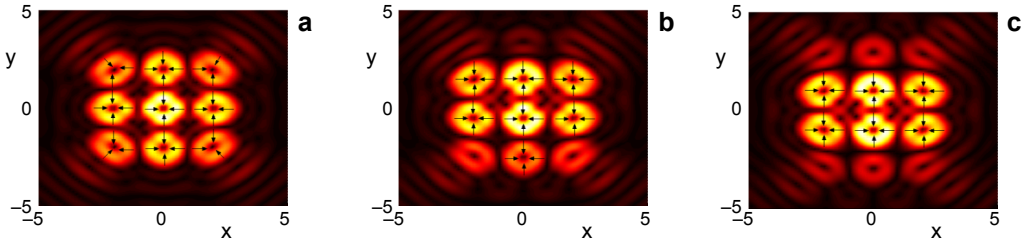

Fig. 7. Gradient force distributions under condition of NA = 0.4, $\beta = 5$, $m = 2$, and $\delta = 0$ (**a**), $\delta = \pi/2$ (**b**) and $\delta = \pi$ (**c**).

$= \beta_y = 5$. Figure 6 illustrates the gradient force distributions for the case of $m = 1$, and it can be seen from this figure that there is one main trap with a weak rhombus force line outside when the phase retardation is zero. On increasing δ, the main force pattern evolution process is very similar, though the force distributions outside differ slightly, by comparing Fig. 5 with Fig. 1. When δ increases up to π, there are two force traps locating along y axis, which shows that the effect of higher β is still obvious.

When the value of the phase factor is chosen as 2, the gradient force is also calculated and shown in Fig. 7. It can be seen by comparing Fig. 7 with Fig. 2 that the effect of the phase factor is very considerable. The gradient force pattern changes remarkably. Under condition of $\delta = 0$, there is a force trap array that consists of nine traps, as shown in Fig. 7**a**, and the difference between Fig. 7**a** and Fig. 2**a** is very distinct. On increasing δ, the whole gradient force distribution shifts along y axis, and the lower trap row weakens sharply. When δ equals π, the lower trap row disappears, and only two trap rows remain. Namely, there are six force traps, and the whole gradient force distribution comes back to be symmetric about x and y axis, as shown in Fig. 7**c**. From this gradient force evolution, we can find that the effect degree of the phase factor on gradient force distribution differs for different m, which should be noted when the tunable gradient force is used in practice in optical systems.

Figure 8 illustrates gradient force distributions for case of $m = 3$. It can be seen that the gradient force distribution is more complex than that shown in Fig. 3, which indicates that higher β leads to gradient force pattern splitting. Many gradient force traps appear and shift along y axis on increasing phase retardation δ. And even when δ increases up to π there are still several obvious gradient force traps in the focal

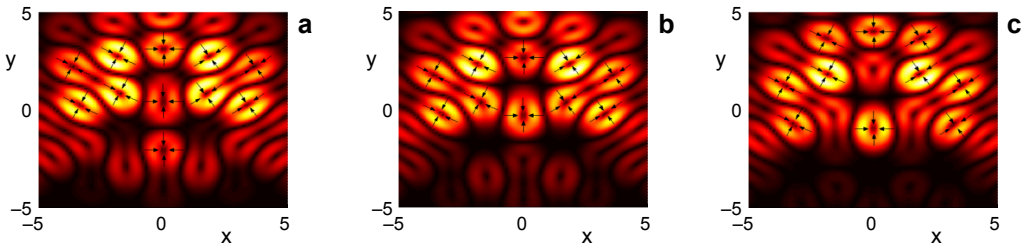

Fig. 8. Gradient force distributions under condition of NA = 0.4, $\beta = 5$, $m = 3$, and $\delta = 0$ (**a**), $\delta = \pi/2$ (**b**) and $\delta = \pi$ (**c**).

plane, as shown in Fig. 8**c**, by comparing Fig. 8 with Fig. 3. Multiple tunable optical traps may come into being under this kind of condition.

We increase the phase factor m continuously up to 4, and the gradient force distributions were calculated and shown in Fig. 9. By comparing Fig. 9 with Fig. 4, we can see that the whole gradient force distributions turn on the force wheel with one center circular gradient force trap under condition of $\delta = 0$. However, for higher β, the gradient force traps outside are more obvious than those in Fig. 4**a**. On increasing the phase retardation δ, the whole gradient force wheel still shifts along y axis, and shrinks in y coordinate direction, and when the value of δ equals π, there remain ten obvious force traps. No obvious gradient force trap disappears in this force pattern evolution.

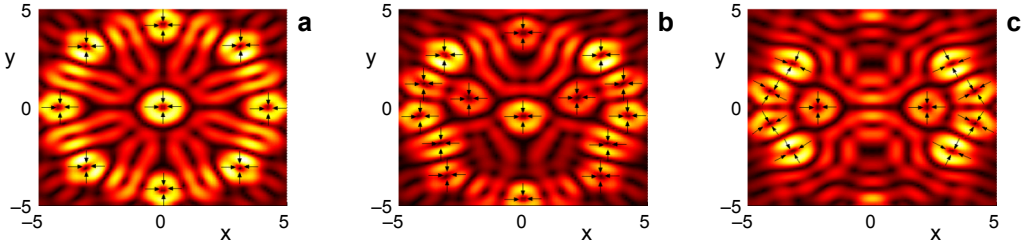

Fig. 9. Gradient force distributions under condition of NA = 0.4, $\beta = 5$, $m = 4$, and $\delta = 0$ (**a**), $\delta = \pi/2$ (**b**) and $\delta = \pi$ (**c**).

Now the value of the phase factor is chosen as 5, gradient force distributions were calculated and shown in Fig. 10. By comparing Fig. 10 with Fig. 5, we can see that there is a very considerable difference between them. Though the whole gradient force pattern still shows pentagon to a certain degree, the strength of those gradient force lines in the negative half-space of y axis become very weak. On increasing the phase retardation δ, the whole gradient force distribution shifts along y axis, and the strength of different gradient force traps fluctuates remarkably. From the above gradient force pattern evolution, higher β may distort the symmetry of gradient force distributions.

From now, the higher numerical aperture condition is considered because the numerical aperture may be higher in some practice optical systems. Here, the numerical

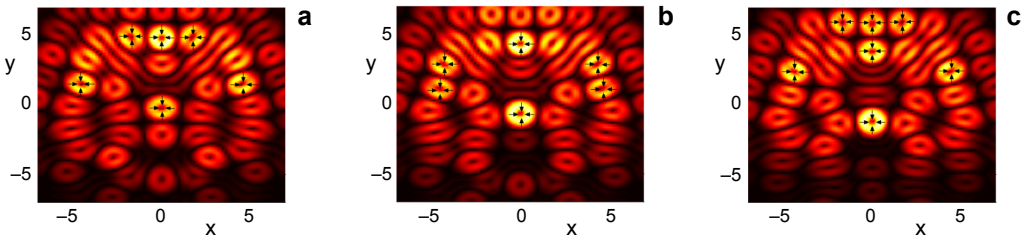

Fig. 10. Gradient force distributions under condition of NA = 0.4, $\beta = 5$, $m = 5$, and $\delta = 0$ (**a**), $\delta = \pi/2$ (**b**) and $\delta = \pi$ (**c**).

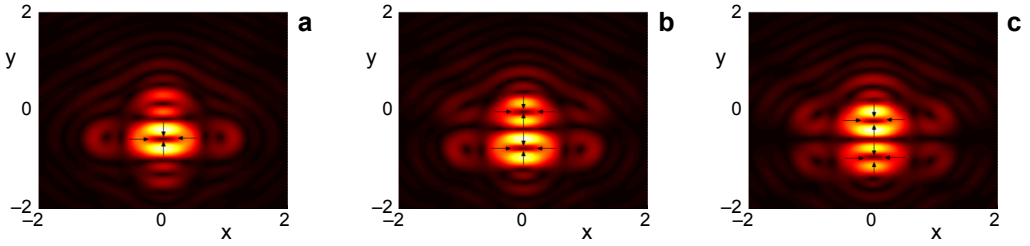

Fig. 11. Gradient force distributions under condition of NA = 0.95, $\beta = 5$, $m = 1$, and $\delta = 0$ (**a**), $\delta = \pi/2$ (**b**) and $\delta = \pi$ (**c**).

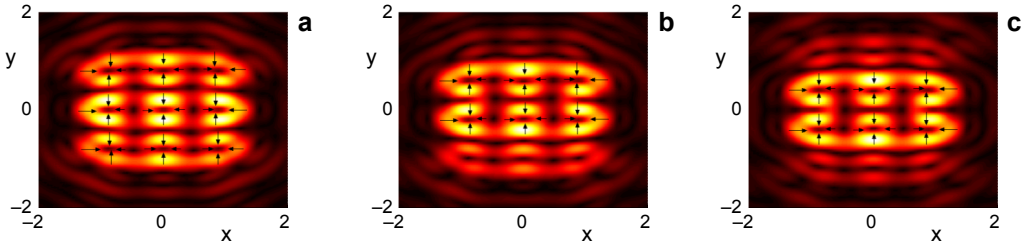

Fig. 12. Gradient force distributions under condition of NA = 0.95, $\beta = 5$, $m = 2$, and $\delta = 0$ (**a**), $\delta = \pi/2$ (**b**) and $\delta = \pi$ (**c**).

aperture is chosen as 0.95. Figure 11 illustrates gradient force distributions under condition of NA = 0.95, $\beta = 5$, and $m = 1$. By comparing Fig. 11 with Fig. 6, it can be seen that the whole gradient force pattern evolution on increasing phase retardation is very similar, and the main difference is that the gradient force shrinks more considerably in y coordinate direction.

When the phase factor increases up to 2, the gradient force is given in Fig. 12. There occurs a remarkable difference between Fig. 12 and Fig. 7. Higher numerical aperture makes the gradient force patterns shrinking in y coordinate direction very evidently, and previous circular gradient force traps change into elliptical shapes with one weak side.

Figures 13 and 14 illustrate the gradient force patterns under condition of $m = 3$ and $m = 4$, respectively. It is also very obvious that higher numerical aperture

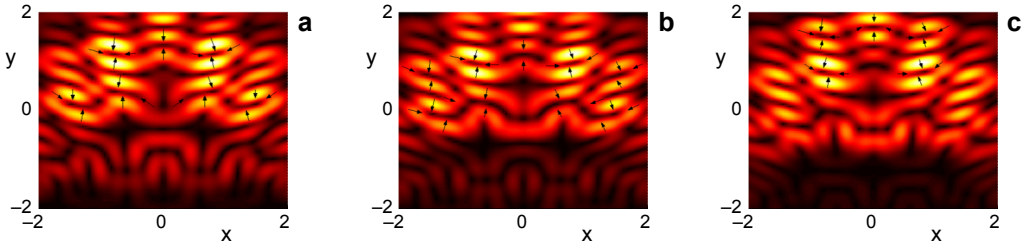

Fig. 13. Gradient force distributions under condition of NA = 0.95, $\beta = 5$, $m = 3$, and $\delta = 0$ (**a**), $\delta = \pi/2$ (**b**) and $\delta = \pi$ (**c**).

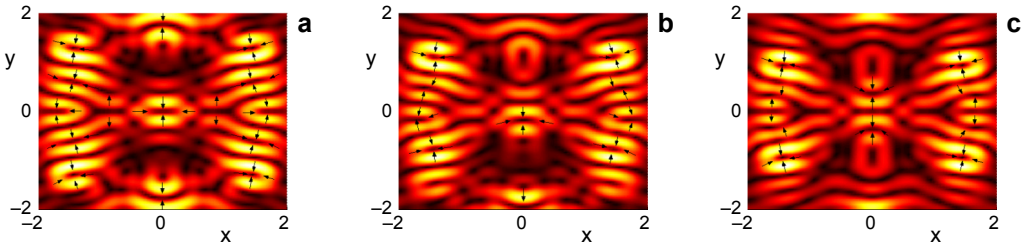

Fig. 14. Gradient force distributions under condition of NA = 0.95, $\beta = 5$, $m = 4$, and $\delta = 0$ (**a**), $\delta = \pi/2$ (**b**) and $\delta = \pi$ (**c**).

compresses the whole gradient force pattern, and some circular force traps distort, so that many scattered force lines come into being.

4. Conclusions

The optical gradient force plays an important role in many optical systems, so the gradient force distributions in the focal plane of cosh-Gaussian beams with sine-azimuthal variation wavefront and half-space phase modulation were investigated in this article. Simulation results show that optical gradient force patterns can be altered considerably by the phase retardation of half-space phase modulation, the phase parameter of azimuthal phase wavefront, beam parameters in cosh terms of the incident beams, and numerical aperture. Some interesting and novel gradient force patterns come into being, including cross-shape, multiple optical trap arrays, multiple-trap wheels, and many kinds of gradient force lines and curves. Symmetry of the whole gradient force pattern can also be changed remarkably.

Acknowledgements – This work was partly supported by Special-Funded Program on National Key Scientific Instruments and Equipment Development (2012YQ17000408), National Natural Science Foundation of China (61378035), Science and Technology Major Project of Zhejiang Province (2012C12017-5), Education Commission of ZheJiang Province of China (Y201120426, Y200803386), and ZHeJiang Province 151 Talent Project of China (12-2-008).

References

[1] POVINELLI M.L., LONCAR M., IBANESCU M., SMYTHE E.J., JOHNSON S.G., CAPASSO F., JOANNOPOULOS J.D., *Evanescent-wave bonding between optical waveguides*, Optics Letters **30**(22), 2005, pp. 3042–3044.

[2] LI M., PERNICE W.H.P., XIONG C., BAEHR-JONES T., HOCHBERG M., TANG H.X., *Harnessing optical forces in integrated photonic circuits*, Nature **456**, 2008, pp. 480–484.

[3] OSKOOI A., FAVUZZI P.A., KAWAKAMI Y., NODA S., *Tailoring repulsive optical forces in nanophotonic waveguides*, Optics Letters **36**(23), 2011, pp. 4638–4640.

[4] MACDONALD M.P., PATERSON L., VOLKE-SEPULVEDA K., ARLT J., SIBBETT W., DHOLAKIA K., *Creation and manipulation of three-dimensional optically trapped structures*, Science **296**(5570), 2002, pp. 1101–1103.

[5] GARCES-CHAVES V., MCGLOIN D., MELVILLE H., SIBBETT W., DHOLAKIA K., *Simultaneous micromanipulation in multiple planes using a self-reconstructing light beam*, Nature **419**, 2002, pp. 145–147.

[6] GRIER D.G., *A revolution in optical manipulation*, Nature **424**, 2003, pp. 810–816.
[7] MACDONALD M.P., SPALDING G.C., DHOLAKIA K., *Microfluidic sorting in an optical lattice*, Nature **426**, 2003, pp. 421–424.
[8] FRIESE M.E.J., NIEMINEN T.A., HECKENBERG N.R., RUBINSZTEIN-DUNLOP H., *Optical alignment and spinning of laser-trapped microscopic particles*, Nature **394**, 1998, pp. 348–350.
[9] PATERSON L., MACDONALD M.P., ARLT J., SIBBETT W., BRYANT P.E., DHOLAKIA K., *Controlled rotation of optically trapped microscopic particles*, Science **292**(5518), 2001, pp. 912–914.
[10] LESTER, M., ARIAS-GONZALEZ J.R., NIETO-VESPERINAS M., *Fundamentals and model of photonic--force microscopy*, Optics Letters **26**(10), 2001, pp. 707–709.
[11] WANG M.D., SCHNITZER M.J., YIN H., LANDICK R., GELLES J., BLOCK S.M., *Force and velocity measured for single molecules of RNA polymerase*, Science **282**(5390), 1998, pp. 902–907.
[12] VISSCHER K., BRAKENHOFF G.J., *Theoretical study of optically induced forces on spherical particles in a single beam trap I: Rayleigh scatterers*, Optik **89**, 1992, pp. 174–180.
[13] TSUTSUI H., HO C.-M., *Cell separation by non-inertial force fields in microfluidic systems*, Mechanics Research Communications **36**(1), 2009, pp. 92–103.
[14] KLIMOV V.V., SEKATSKII S.K., DIETLER G., *Laser nanotraps and nanotweezers for cold atoms: 3D gradient dipole force trap in the vicinity of scanning near-field optical microscope tip*, Optics Communications **259**(2), 2006, pp. 883–887.
[15] GAO X., ZHOU F., XU W., GAN F., *Gradient force pattern, focal shift, and focal switch in an apodized optical system*, Optik **116**(3), 2005, pp. 99–106.
[16] LI J., ZHUANG S., HUANG C., *Gradient force evolution of Gaussian beam induced by a phase plate*, Optics and Lasers in Engineering **46**(8), 2008, pp. 595–600.
[17] FONG K.Y., PERNICE W.H.P., LI M., TANG H.X., *Tunable optical coupler controlled by optical gradient forces*, Optics Express **19**(16), 2011, pp. 15098–15108.
[18] LÜ B., ZHANG B., MA H., *Beam-propagation factor and mode-coherence coefficients of hyperbolic--cosine Gaussian beams*, Optics Letters **24**(10), 1999, pp. 640–642.
[19] EYYUBOGLU H.T., BAYKAL Y., *Average intensity and spreading of cosh-Gaussian laser beams in the turbulent atmosphere*, Applied Optics **44**(6), 2005, pp. 976–983.
[20] HRICHA Z., BELAFHAL A., *Focusing properties and focal shift in hyperbolic-cosine-Gaussian beams*, Optics Communications **253**(4–6), 2005, pp. 242–249.
[21] GAO X., *Focusing properties of the hyperbolic-cosine-Gaussian beam induced by phase plate*, Physics Letters A **360**(2), 2006, pp. 330–335.
[22] CHU X., NI Y., ZHOU G., *Propagation of cosh-Gaussian beams diffracted by a circular aperture in turbulent atmosphere*, Applied Physics B **87**(3), 2007, pp. 547–552.
[23] DONG X., ZHAN Q., GAO X., GENG T., GUO H., ZHUANG S., *Hyperbolic-cosine-Gaussian beam with sine-azimuthal variation wavefront*, Optik **123**(21), 2012, pp. 1901–1906.
[24] PATIL S.D., NAVARE S.T., TAKALE M.V., DONGARE M.B., *Self-focusing of cosh-Gaussian laser beams in a parabolic medium with linear absorption*, Optics and Lasers in Engineering **47**(5), 2009, pp. 604–606.
[25] PATIL S.D., TAKALE M.V., NAVARE S.T., FULARI V.J., DONGARE M.B., *Relativistic self-focusing of cosh-Gaussian laser beams in a plasma*, Optics and Laser Technology **44**(2), 2012, pp. 314–317.
[26] GAO X., WANG J., GU H., HU S., *Focusing of hyperbolic-cosine-Gaussian beam with a non-spiral vortex*, Optik **120**(5), 2009, pp. 201–206.
[27] GAO X., ZHAN Q., LI J., HU S., WANG J., ZHUANG S., *Dark focal spot shaping of hyperbolic-cosine--Gaussian beam*, Journal of the Optical Society of America B **27**(4), 2010, pp. 696–702.
[28] GAO X., WANG Q., ZHAN Q., YUN M., GUO H., ZHUANG S., *Focal patterns of higher order hyperbolic--cosine-Gaussian beam with one optical vortex*, Optical and Quantum Electronics **42**(6–7), 2011, pp. 369–380.
[29] LIAN X., LÜ B., *Phase singularities of nonparaxial cosh-Gaussian vortex beams diffracted by a rectangular aperture*, Optics and Laser Technology **43**(7), 2011, pp. 1264–1269.

[30] GAO X., LI Z., WANG J., SUN L., ZHUANG S., *Tunable gradient force of hyperbolic-cosine-Gaussian beam with vortices*, Optics and Lasers in Engineering **48**(7–8), 2010, pp. 766–773.
[31] GU M., *Advanced Optical Imaging Theory*, Springer, Heidelberg, 2000.
[32] GANIC, D. GAN X., GU M., *Focusing of doughnut laser beams by a high numerical-aperture objective in free space*, Optics Express **11**(21), 2003, pp. 2747–2752.

Received February 17, 2013